# Cyclobutane-based peptides / terpyridine conjugates: Their use in metal catalysis and as functional organogelators[#]

**Oriol Porcar-Tost, Bernat Pi-Boleda, Jordi García-Anton, Ona Illa,***

**Rosa M. Ortuño***

*Departament de Química, Universitat Autònoma de Barcelona, 08193 Cerdanyola del Vallès, Barcelona, Spain.*

## ABSTRACT

Two new conjugates, hcptpyDP and hcptpyTP, of a terpyridine derivative incorporating artificial peptide moieties, have been synthesized and their use in the preparation of metal catalysts and organogelators has been investigated. Ru(II) complexes derived from these ligands showed electrochemical behavior and activity as catalysts in the epoxidation of olefins similar to that of Beller's catalyst. As organogelators, these conjugates were able to gelate a variety of solvents, from toluene to methanol, with satisfactory *mgc* (minimum gelation concentration) values. The presence of 4'-(4-carboxy)phenylterpyridine (hcptpy) moiety allows tuning the gelling properties and also influences the supramolecular self-assembling mode to produce chiral aggregates with respect to parent peptides DP and TP. In the case of the conjugates, π–π interactions provided by the aromatic moieties cooperate with inter-molecular hydrogen bonding between N*H* and C*O* in the amide groups. Further properties of peptide / terpyridine conjugates are under investigation in view of future applications.



*Key words:*

Terpyridine conjugates

Cyclobutane-based peptides

Ruthenium complexes

Metal catalysis

Functional organogelators

## 1. Introduction

Since its isolation in 1932[1] from a mixture of the oxidative coupling products of pyridine, 2,2':6',2''-terpyridine (tpy) has been considered as one of the most well-liked tridentate ligands in chemistry. Its strong coordination ability towards metal ions enables terpyridine to be used as a ligand for the preparation of catalysts in several reactions.[2,3] In addition, terpyridine and derivatives play a key role as supramolecular building blocks and, consequently, they are valuable for the elaboration of metallopolymers, switching devices, light-harvesting systems, and artificial photosynthetic models, among other purposes.[3,4]

Later, the use of terpyridine conjugates constituted a growing research field trying to enhance or tune the properties of terpyridine itself and to find new applications. For instance, Cu(II)-terpyridine conjugates were used for biological applications.[5] Moreover, Ru(II)-terpyridine conjugates have been used in dye-sensitized solar cells[6] while Pt(II)-terpyridine acetylide complexes have been investigated with the objective of photogeneration of hydrogen in aqueous media.[7] Very recently, arylene-vinylene terpyridine conjugates revealed their ability as chemosensors performing as fluorescent probes[8] and highly luminescent π-conjugated terpyridine derivatives exhibited thermally activated delayed fluorescence (TDAF) owning very promising properties to be applied in the development of supramolecular systems and sensors.[9] Besides, the terpyridine derivative 4'-(4-carboxyphenyl)-2,2':6',2''-terpyridine (hcptpy) has been used in the development of compounds for biomedical applications,[10] and photoelectronic devices and sensors including gels,[11] metal-organic frameworks (MOF),[12] and metal-organic gels (MOG).[13]

All these properties confer terpyridine derivatives with an enormous potential for the design of new catalysts and molecular or supramolecular materials for manifold purposes.

Regarding supramolecular materials,[14] functional organogels constitute a family of soft materials[15] with diverse utilities. Some of their applications include products for industrial purposes and fine chemicals as well as their use in biomedicine and materials science.[16,17] Very recently, their potential as materials for environmental remediation[18] and oil spill recovery[19] has been reported.

We have described the properties and mode of aggregation of peptide based organogels containing artificial cyclobutane β-amino acids,[20,21] as well as hybrid peptides that result from the combination of cyclobutane β-monomers with linear residues.[22] The behavior of cycloalkane bisamides has also been investigated accounting for the effect of regiochemistry and stereochemistry on the supramolecular self-assembly. Interestingly, we have afforded new examples on stochastic chiral symmetry breaking induced by sonication, which allowed the formation of chiral aggregates from meso achiral molecules.[23]

In this paper, we report the preparation of new terpyridine conjugates hcptpyDP and hcptpyTP that result of combining the hcptpy moiety with a cyclobutane-based dipeptide (DP) and a tetrapeptide (TP), respectively, shown in Scheme 1. The aim of this work lies on two main aspects: one of them is the investigation of the influence of the peptide backbone on the properties of a Ru(II)-tpy complex as a catalyst in the oxidation of olefins. The new Ru(II) complexes have been characterized and their redox properties have been compared with similar complexes from terpyridine itself. The second objective consists in the study and rationalization of the contributions exerted by the flat π-electron rich terpyridine moiety and the chiral peptide subunit, which is prone

to hydrogen bonding through the amide groups, to the hierarchical supramolecular organization of these conjugates into gels. The results of this study have been compared with the properties of the parent peptides DP and TP and have been supported by computational calculations.

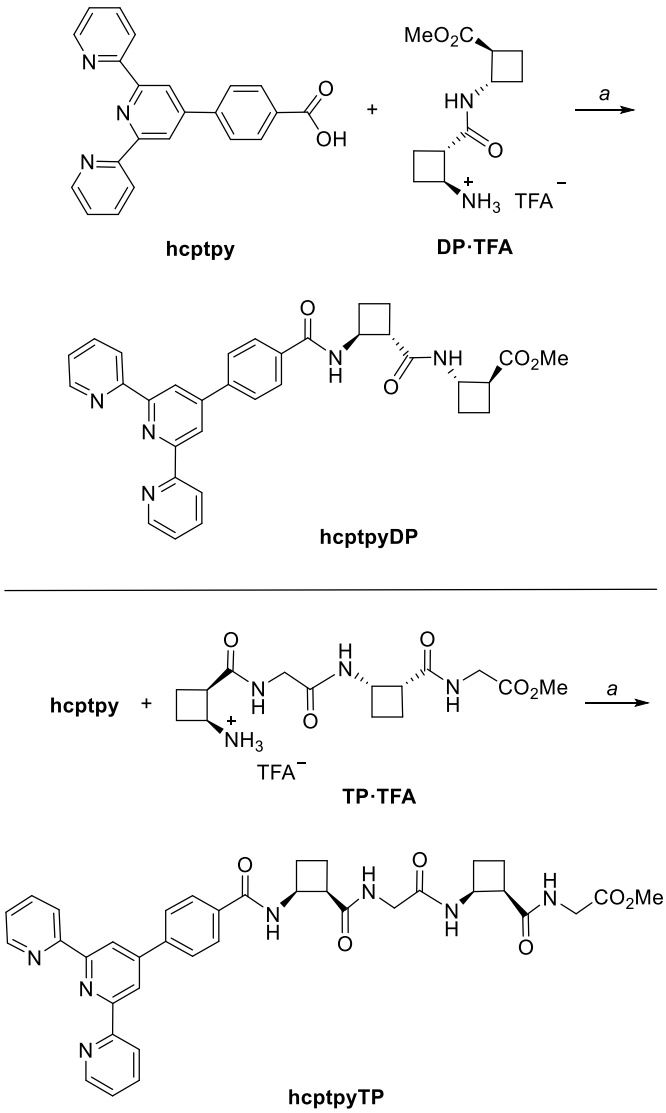


**Scheme 1.** Synthesis of conjugates hcptpyDP and hcptpyTP

## 2. Results and discussion

### 2.1 Synthesis of terpyridine-peptide conjugates.

The terpyridine moiety was conjugated to dipeptide DP[24] and tetrapeptide TP,[25] respectively, by coupling with hcptpy[26] using FDPP (pentafluorophenyl diphenylphosphinate) and DIPEA (*N*,*N*-diisopropylethylamine) in anhydrous DMF, at room temperature for 18 h. In this way, conjugates hcptpyDP and hcptpyTP were prepared in 60-65% yield (Scheme 1).

### 2.2 Preparation of the Ru(II) complexes [Ru(pydic)(hcptpyDP)] and [Ru(pydic)(hcptpyTP)], electrochemical characterization and their use in catalyzed olefin epoxidation

Since $Ru(tpy)_2$ complexes are quite inert and usually do not have applications in catalysis,[27] pyridine-2,6-dicarboxylate (pydic) was used as the second ligand in the complex.

The syntheses of the ruthenium complexes [Ru(pydic)(hcptpyDP)] and [Ru(pydic)(hcptpyTP)], were achieved in one step in 54-60% yield by reacting one equivalent of hcptpyDP or hcptpyTP with one equivalent of pydic ligand and one equivalent of Ru(*p*-cymene)$Cl_2$, in refluxing methanol-water (Scheme 2). Due to their high stability, both complexes were purified by column chromatography and characterized using common techniques.

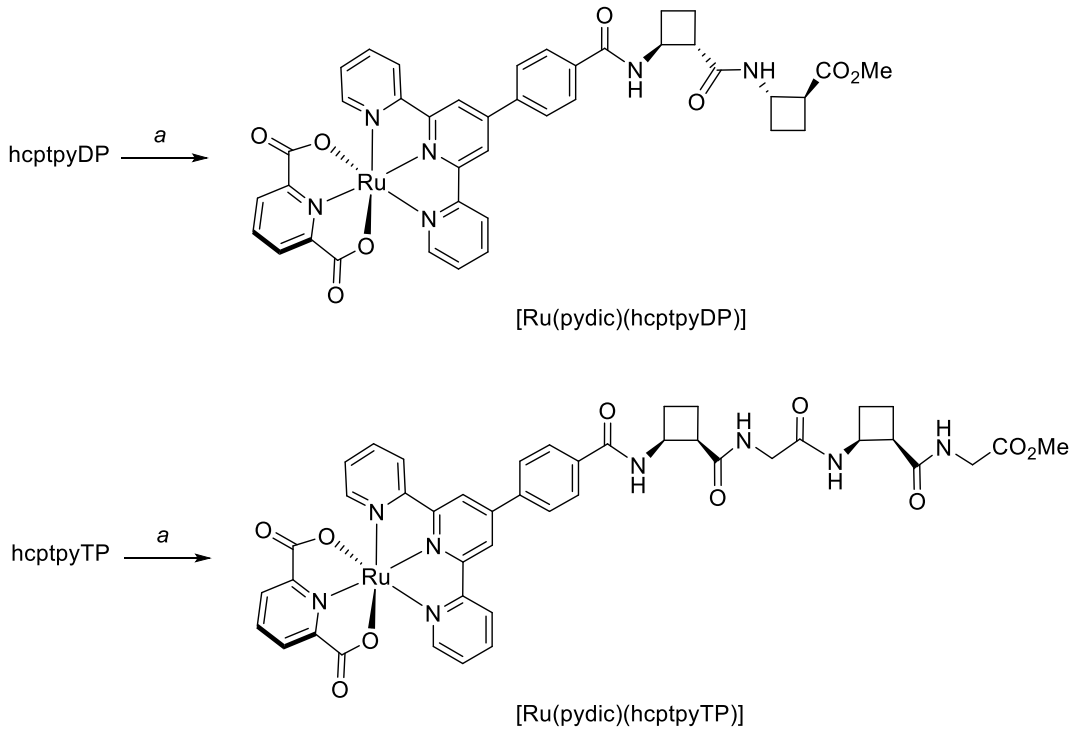


Reagents and conditions. *a*: pydic, Ru(*p*-cymene)$Cl_2$, MeOH-$H_2O$, reflux, 18 h. 54-60%

**Scheme 2.** Synthesis of complexes [Ru(pydic)(hcptpyDP)] and [Ru(pydic)(hcptpyTP)].

Electrochemical studies of Ru(II) complexes were undertaken to understand the redox properties of these compounds. These results are interesting for catalytic applications where an oxidation or reduction step is required. The methodologies used were cyclic voltammetry (CV) (Fig. 1) and differential pulse voltammetry (DPV) in methanol (Fig. S1 in the Supplementary Data). This solvent is not often used in electrochemistry because its electrochemical window is not wide. Nevertheless, it was not electroactive in the considered potential range allowing studying the oxidation potential of the complexes. $TBABF_4$ was used as supporting electrolyte.

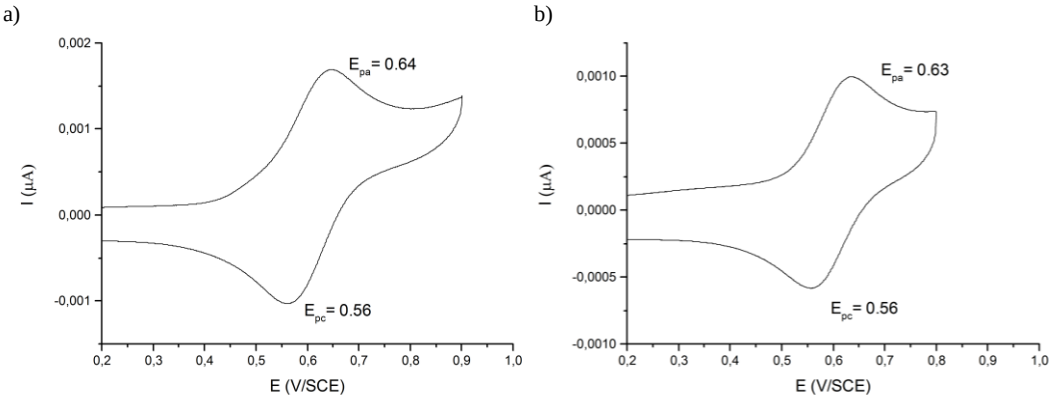


**Fig. 1.** CV voltammograms for (a) 7 mM [Ru(pydic)(hcptpyDP)] and (b) 7 mM [Ru(pydic)(hcptpyTP)], and 0.1 M $TBABF_4$ solution in methanol. Glassy carbon working electrode, Pt counter electrode and SCE reference electrode. v = 0.1 V/s.

Both complexes were redox active. The CV voltammograms exhibited one reversible oxidation wave associated with the Ru(II) to Ru(III) redox couple. Determination of $E_{1/2}$ (half-wave potential) has been made by using the equations described in the Supplementary Data and the resulting values are shown in Table 1 where the $E_{1/2}$ value of the related complex [Ru(pydic)(tpy)] (Beller's catalyst) described in the literature[2] is also shown for comparison.

**Table 1**. $E_{1/2}$ values for complexes **[**Ru(pydic)(hcptpyDP)], [Ru(pydic)(hcptpyTP)] and **[**Ru(pydic)(tpy)] using CV and DPV

| **Complex** | **$E_{1/2}$ (CV)** | **$E_{1/2}$ (DPV)** |
|---|---|---|
| [Ru(pydic)(hcptpyDP)] | 0.600 V | 0.585 V |
| [Ru(pydic)(hcptpyTP)] | 0.595 V | 0.565 V |
| [Ru(pydic)(tpy)][2] | 0.600 V | - |

The observed $E_{1/2}$ values are due to the oxidation of Ru(II) and are essentially the same using both CV and DPV techniques. The presence of the peptide moiety in [Ru(pydic)(hcptpyDP)] and [Ru(pydic)(hcptpyTP)] does not alter the oxidation of the metal ion because it is located at a considerably distant position from the coordination sphere of the ruthenium ion. Since these complexes have a $E_{1/2}$ value close to [Ru(pydic)(tpy)], a comparable reactivity was expected for all three catalysts.

The epoxidation of styrene, **1** (R = H), and derivatives, **1** (R = Me, Ph), was chosen as a process to test the ability of the synthesized complexes in oxidation reactions (Scheme 3). Conditions were similar to those described in the literature for the oxidation of styrenes by using Beller's catalyst.[2]

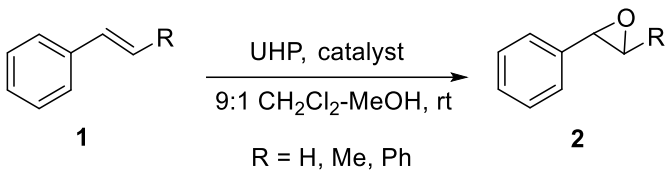


**Scheme 3.** Epoxidation of styrene and derivatives, **1,** using complexes [Ru(pydic)(hcptpyDP)] or [Ru(pydic)(hcptpyTP)] as catalyst.

Complexes [Ru(pydic)(hcptpyDP)] and [Ru(pydic)(hcptpyTP)] are insoluble in common organic solvents but they are soluble in high polar ones such as MeOH, DMF or DMSO. However, the use of methanol as the only solvent was precluded since methanolysis of the produced epoxide **2** was observed. Thus, reactions were carried out in a 9:1 $CH_2Cl_2$ - MeOH mixture and using UHP (urea hydrogen peroxide) as the oxidant agent, at room temperature. Results are shown in Table 2 where data from the literature[2] are also described for comparison.

**Table 2**. Epoxidation of styrene and derivatives by using ruthenium complexes [Ru(pydic)(hcptpyDP)], [Ru(pydic)(hcptpyTP)] and $[Ru(pydic)(tpy)]^2$ as catalysts

| Complex | Substrate 1, R | Yield (%)[a] | Time (h) |
|---|---|---|---|
| [Ru(pydic)(hcptpyDP)] | H | 60 | 2.5 |
| | Ph | 97 | 7 |
| | Me | 99 | 5 |
| [Ru(pydic)(hcptpyTP)] | H | 48 | 3.5 |
| | Ph | 90 | 8 |
| | Me | 98 | 5 |
| $[Ru(pydic)(tpy)]^2$ | H | 39 | 3 |
| | Ph | 99 | 1 |
| | Me | 99 | 3 |

All reactions were carried out using 0.5 mmol of substrate in 10 mL of 9:1 dichloromethane-methanol as solvent. [a] Yields determined by GC analysis

Results showed that both complexes are able to catalyze the formation of the epoxidation product in moderate yields in the case of styrene, and excellent yields using other substituted substrates. Catalyst [Ru(pydic)(hcptpyDP)] gave slightly better yields and shorter reaction times than [Ru(pydic)(hcptpyTP)] in the case of styrene, **1** (R = H), and *trans*-stilbene, **1** (R = Ph). This result can be justified by the fact that, with long reaction times, solvolysis of the produced epoxide can occur since methanol is used as co-solvent**.** Beller's catalyst gave similar yields but faster reactions in the case of *trans*-stilbene and β-methyl styrene, **1** (R = Me), but lower yield in the case of styrene. These results are in agreement with the electrochemical studies described above, which predicted similar reactivity for all complexes.

Unfortunately, epoxidation products were obtained in racemic form. This result shows that the chiral peptide moiety is too far from the catalytic center to induce any asymmetry during the process.

### 2.3 Gelation studies on conjugates hcptpyDP and hcptpyTP. Comparison with the parent peptides DP and TP

**Formation of gels.** The gelation ability of hcptpyDP and hcptpyTP was studied in thirteen solvents of different polarity. The tube inversion test was used to determine the formation of a gel, following the procedure described in the Experimental Section. Organogelators hcptpyDP and hcptpyTP, as well as peptides DP and TP were insoluble in very apolar solvents, such as pentane, and also in water. Macroscopically, the gels formed by hcptpyDP and hcptpyTP in alcohols are opaque, while the gels formed in the other solvents are translucent.

All gels reported herein were stable at room temperature, at least, for one month. Furthermore, they were thermoreversible. As an example, two images of the sol-gel transition of a gel formed by hcptpyTP in methanol are shown in Fig. 2. The thermoreversibility is an evidence that the aggregates formed by these organogelators are physical gels assembled by non covalent intermolecular bonds. A study of their aggregation mode is described below.

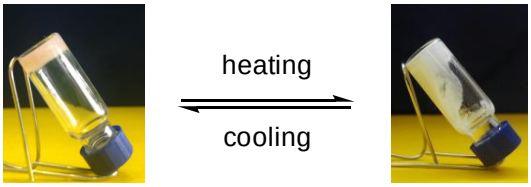


**Fig. 2.** Thermoreversibility of the gel formed by hcptpyTP in methanol.

Results were quantified by the minimum gelation concentration (*mgc*). In order to compare the gelling ability of hcptpyDP and hcptpyTP as well as the effect of the introduced terpyridine moiety, the results obtained for peptides DP[21] and TP[22] are also shown in Table 3.

**Table 3.** Gelation study[a] of hcptpyDP and hcptpyTP compared with DP[21] and TP[22] in common solvents[a] Solvent and minimum gel concentration[b,c]

| Gelator | 1,4-Dioxane | Toluene | $CHCl_3$ | *tert*-AmOH | AcOEt | THF | DCM | iso-PrOH | Acetone | MeOH | AcCN |
|---|---|---|---|---|---|---|---|---|---|---|---|
| hcptpyDP | s | 49 (87) | 84 (150) | 123 (217) | 100 (178) | 104 (185) | 100 (178) | 78 (139) | 58 (103) | 59 (105) | 76 (135) |
| DP[21] | s | 6 (27) | s | s | 33 (146) | 112 (495) | s | s | 80 (354) | s | 57 (251) |
| hcptpyTP | 114 (169) | 63 (93) | s | 67 (99) | 92 (136) | 79 (117) | s | 43 (64) | 104 (154) | 48 (71) | i |
| TP[22] | 33 (97) | 3 (9) | 122 (358) | s | 8 (24) | 100 (294) | 60 (176) | 50 (147) | 50 (147) | 100 (294) | 17 (50) |

[a] Solvents are ordered by increasing dielectric constant. [b] *mgc* in mg $mL^{-1}$ and, in parentheses, mM. [c] S: soluble, I: insoluble

For hcptpyDP, the lowest *mgc* values found were 49, 58 and 59 mg $mL^{-1}$, corresponding to toluene, acetone and methanol, respectively. Interestingly, although some *mgc* values are higher than those for the same solvents with DP as organogelator, hcptpyDP can gelate a broader range of solvents including apolar dichloromethane and protic polar solvents such as methanol and *tert*-amyl alcohol.

Although hcptpyTP is insoluble in acetonitrile and it is soluble in chloroform and dichloromethane, it can gelate the other eight solvents tested. The best *mgc* values found are 43 and 48 mg $mL^{-1}$, corresponding to isopropanol and methanol, respectively, which

are also gelated by TP but with higher *mgc* values. The values for the other solvents are in the range of 63 and 104 mg $mL^{-1}$.

**Scanning Electron Microscopy (SEM).** SEM experiments were undertaken to investigate the aggregates formed by of hcptpyDP and hcptpyTP both in toluene and methanol. Selected micrographs are shown in Fig. 3 and revealed a remarkable influence of the solvent nature on the morphology of the supramolecular aggregates. Xerogels of hcptpyDP from methanol show undefined structures. In higher magnifications, it looks like squashed fibers. On the other hand, disordered bundles of fibers are observed, with lengths of 120 to 200 nm, for the xerogel formed from toluene.

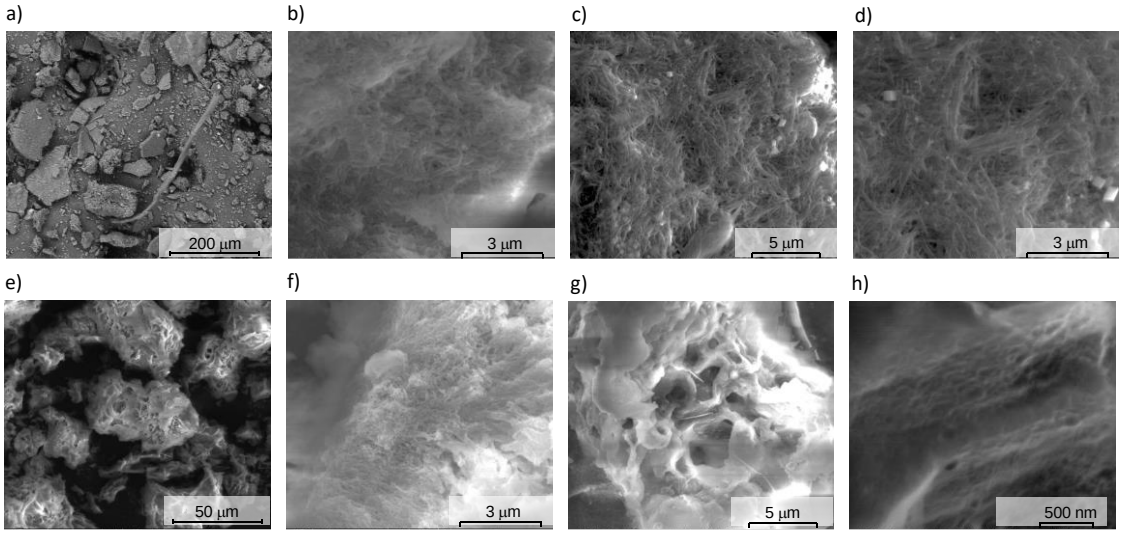


**Fig. 3.** SEM micrographs of xerogels produced by a, b) hcptpyDP from methanol; c, d) hcptpyDP from toluene; e, f) hcptpyTP from methanol; g, h) hcptpyTP from from toluene. Two magnifications are shown in each case.

Xerogels of hcptpyTP from methanol exhibit an undefined spongy structure whose cavities are formed by smashed fibers, as can be observed in higher magnifications. Besides, xerogels formed by hcptpyTP in toluene present undefined structures. In higher magnifications, however, we can notice that the walls of this structure are made of

regular fibers of around 40 nm. By comparison of these micrographs with those for the parent peptides we can conclude that the xerogels from DP[21] and TP[22] present better defined and more regular structures in the form of fibers. An explanation for this difference could be that the presence of the 4'-phenylterpyridine moiety disrupts the self-assembly pattern of the molecules regarding the peptide backbone and imposes other type of interactions, i.e. electronic π–π interactions, which also contribute to the hierarchical self-assembly in whole.

**Computational calculations on the aggregation mode**. Calculations were carried out to better understand the structure of the gels, their formation process and to establish the main interactions responsible for the supramolecular arrangement. The aggregation energies of hcptpyDP and hcptpyTP were compared with the aggregation energies of dipeptide DP and tetrapeptide TP, to understand whether the 4'-phenylterpyridine moiety benefits the aggregation in energetic terms or not.

A conformational search of hcptpyDP and hcptpyTP as single molecules was carried out by using molecular mechanics. Then, the most stable structures obtained were optimized employing quantum mechanics using M06-2X as DFT functional (Fig. 4). In the resulting computed geometries, we can observe that the structure of hcptpyDP is extended and fixed by an eight-membered hydrogen-bonded ring which is typical for *trans*-based cyclobutane moieties.[24,28] On the other hand, the structure of hcptpyTP is folded and fixed by three hydrogen bonds between the carbonyl oxygen atoms (C*O*) and the N*H* protons of different amide groups. The relative conformation of the peptide moieties in hcptpyDP and hcptpyTP are the same found in previous studies of DP and TP**,**[24,28] so the incorporated 4'-phenylterpyridine unit does not play a significant role.

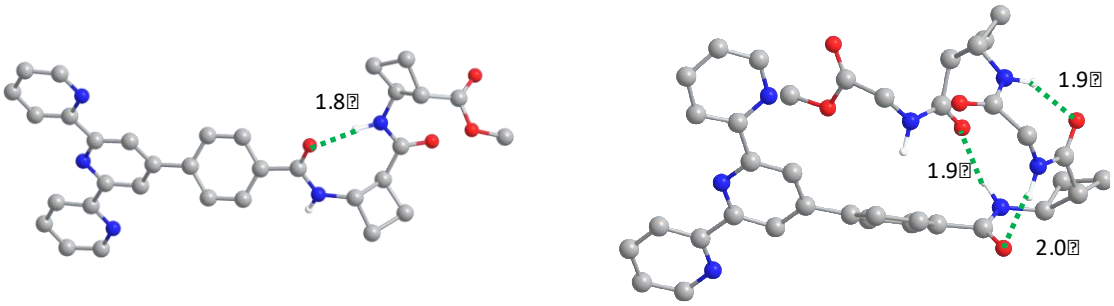


**Fig. 4.** Optimized structures of hcptpyDP (left) and hcptpyTP (right). Hydrogen bonds are remarked with green lines. Distances are in Å.

Once the structure of the discrete molecules was computed, their small aggregates were studied. The conformational search performed for dimeric and tetrameric aggregates of both compounds showed that the most stable structures involved intermolecular hydrogen bonds between the N*H* groups of one molecule and the C*O* groups of the other one. These hydrogen bonds may be formed in two different directions, head-to-head and head-to-tail. The head-to-head arrangement was the most favorable in all cases (see Table 1 in ESI) and is shown in Fig. 5.

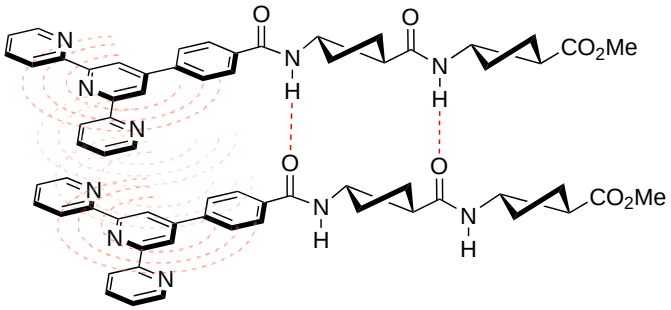


**Fig. 5.** Schematic representation of head-to-head arrangement of a dimer of conjugate hcptpyDP. π-π and H-bonding interactions are highlighted in red.

Results of calculations showed that the aggregation energies are more favorable when the number of monomers increased. Also, the aggregation energy per molecule increases in all cases, and it could mean that the self-assembly of both compounds is

promoted by a cooperative effect.[29] $\Delta E_{agg}$ for tetrameric aggregate of DP is -59 kcal/mol while it is -113 kcal/mol for hcptpyDP. Likewise, $\Delta E_{agg}$ for the TP tetramer is -51 kcal/mol while it is -136 kcal/mol for tetrameric hcptpyTP. By comparing these values, we can conclude that the terpyridine substructure plays an important role in the aggregation process.

Optimized structures of the dimeric and tetrameric aggregates show that conjugates hcptpyDP and hcptpyTP self-assemble in a preferred monodirectional dimension and that terpyridine moieties are in a parallel disposition (Fig. 6).

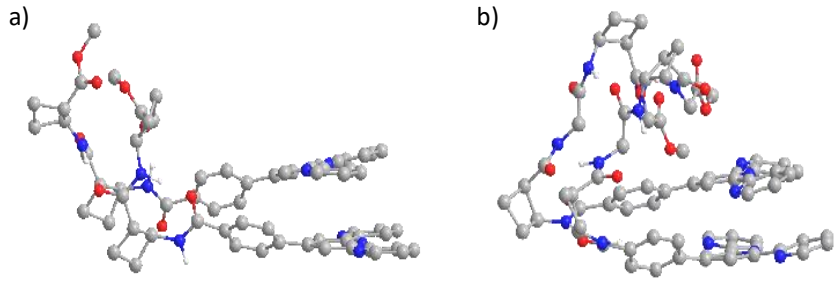


**Fig. 6.** Side view of the predicted structure of a dimeric aggregate of a) hcptpyDP and b) hcptpyTP. Non-polar H atoms were omitted for clarity.

When the aggregates grow, a helical-like structure is observed. This effect is more marked for hcptpyTP than for hcptpyDP because the peptide moiety of the former is larger, thus more flexible, and its accommodation in a helical-like aggregate is easier. For this reason, only the formation of aggregates from hcptpyTP was considered.

The dodecameric structure of hcptpyTP was constructed using the same methodology described for the dimer and tetramer but, in this case, only a minimization of the energy using molecular mechanics was carried out. The helical trend was confirmed (Fig. 7).

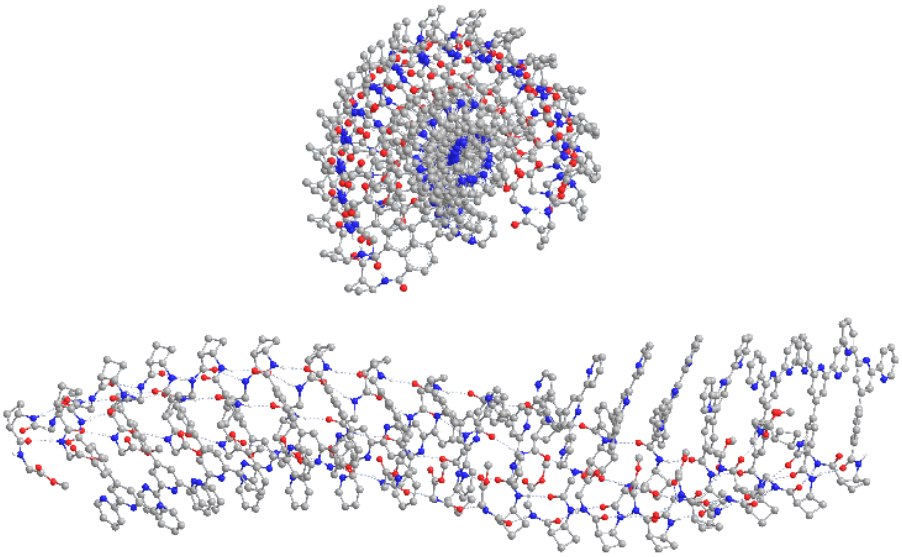

**Fig. 7.** Top and side view for the predicted structure of a dodecameric aggregate of hcptpyTP. Non-polar H atoms were omitted for clarity.

Looking at the aggregate from a top view, we can see the relative position of the 4'-phenylterpyridine moieties and the peptide skeletons along the fibril. Interestingly, while the aromatic moieties remain in the middle of the fibril, the peptide backbone of the molecules spins around. Thus, to clarify the exact position of each function in the big aggregate, the dodecamer was cut and an internal dimer and monomer were extracted (Fig. 8). We can observe that each amide group of the compound forms hydrogen bonds with the equivalent amide group of the next molecule. So, each molecule that participates into the supramolecular aggregate establishes four hydrogen bonds with the next molecule. It is remarkable that similar results had been obtained for the structure of hexadecameric aggregate of tetrapeptide TP.[22]

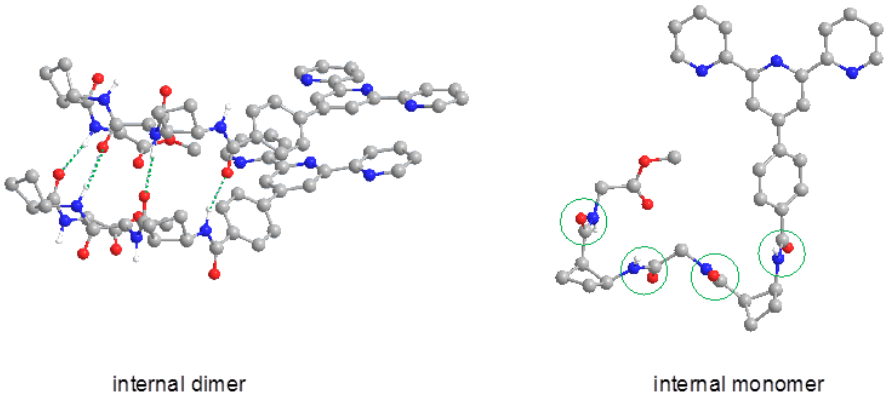


**Fig. 8.** Internal dimer and monomer of the dodecameric aggregate of hcptpyTP. Hydrogen bonds in the dimer and amide groups in the monomer are remarked in green. Non-polar H atoms were omitted for clarity.

Similar results were obtained for hcptpyDP. Accordingly, calculations of big aggregates suggest that the 4'-phenylterpyridine moiety in conjugates hcptpyDP and hcptpyTP does not interphere in the interactions of the peptide part. Furthermore, each pyridine and phenyl ring remains in a shifted parallel position due to π-stacking interactions with the equivalent functions of the following and the previous molecule. These predictions from calculations were confirmed by data from circular dichroism and UV studies.

**Circular Dichroism (CD) and UV spectroscopies.** As expected, the UV spectra of compounds hcptpyDP and hcptpyTP show two differentiated parts corresponding to the aromatic 4'-phenylterpyridine substructure (250-280 nm) and the amide absorption (200 nm), respectively (See Figure S2 in Supplementary Data).

CD spectra were recorded for hcptpyDP and hcptpyTP in methanol solution and as xerogels from toluene (Fig. 9).

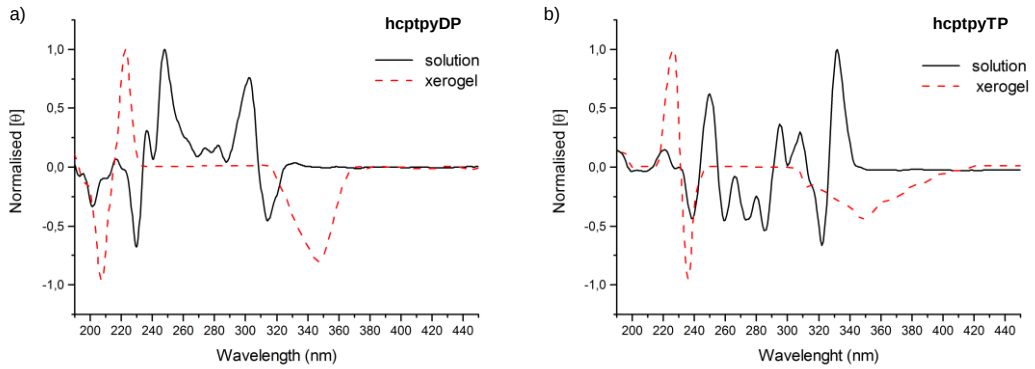


**Fig. 9.** Normalized CD spectra of a) conjugate hcptpyDP and b) conjugate hcptpyTP in 0.05 mM solutions in MeOH and as xerogels at the *mgc* from toluene in KBr (0.02 mmol/g).

In contrast to the spectra in solution, which are rather complicated, the spectra of xerogels appear simplified and are similar for both compounds. Thus, a bisignate signal with zero crossing at 217 (225) nm and a broad signal at 247 (252) nm are observed, for hcptpyDP (hcptpyTP), respectively. The bisignate signal can be attributed to the amides and has shifted to shorter wavelengths with respect to the equivalent signal in solution. This blue shift is related to the difference between the intramolecular hydrogen bonds of the amide groups in solution and the intermolecular hydrogen bonds in the aggregate. Moreover, the shape of the signal is bisignate, indicating that the relative position of the amides in the aggregate is not symmetrical. This behavior is typically described for helical aggregates.[23,30] Concerning the signal of the aromatic functions, in xerogel phase it has shifted to higher wavelength and its chirality has changed from a bisignate signal in solution to a broad band in the aggregate. The single band could be explained because the relative position of the aromatic functions is parallel between them, as it is shown in the calculated structure. The red shift of the band due to the aromatic functions could be related to partial overlapping of them, performing a kind of staircase aggregation, as

observed in many examples of aggregates of aromatic compounds, such as porphyrins.[31] Moreover, in the case of hcptpyTP, the relative position of the amide groups between the molecules are non-parallel, generating helicity, while the aromatic groups remain in a shifted parallel plane. These interpretations constitute another evidence of the helical-like structure of the aggregates found by calculations. Also, bigger aggregates of these compounds could form fibers, which is in accordance with the SEM experiments.

## 3. Conclusions

Two new conjugates of terpyridine incorporating peptide moieties have been prepared. On one hand, these compounds were used as ligands for the preparation of Ru(II) complexes whose behavior as catalysts for epoxidation of phenyl-substituted olefins was explored. Results showed that the efficiency in catalysis is similar to that of previously described [Ru(pydic)(tpy)] complex. Unfortunately, epoxides were obtained in racemic form in all cases studied, probably due to the long distance between the catalytic center and the chiral peptide moiety that would adopt a not enough folded conformation of the ligand. More promising were the results from the investigation of hcptpyDP and hcptpyTP as organogelators. They can gelate a broad diversity of solvents from aromatics, to aprotic polar and protic polar solvents, with satisfactory *mgc* values. Actually, it seems that π–π interactions between the terpyridine substructures and hydrogen bonding between the amide groups of the peptides in different molecules have a cooperative effect in the supramolecular arrangement to self assemble into the corresponding aggregates. Their morphology is strongly solvent-dependent as shown by SEM. For instance, in toluene, they afford helical aggregates as verified by CD spectroscopy and explained by computational calculations. With these results in hand,

further properties of hcptpy-peptide conjugates are under investigation in view of future applications.

## 4. Experimental

### *4.1 General Information*

The chemicals and reagents were of analytical grade and were used without further purification. Anhydrous solvents were freshly distilled when needed under nitrogen atmosphere. Flash chromatography purifications were carried out on silica gel (200-400 mesh). Melting points were recorded on a Reicher Klofler block and values are uncorrected. $^{1}$H NMR and $^{13}$C NMR spectra were measured in an ARX 400 Bruker apparatus ($^{1}$H at 400MHz, $^{13}$C at 100 MHz) in $CDCl_3$ or DMSO-$d_6$ solutions. IR spectra were obtained from samples in neat form with an Attenuated Total Reflectance (ATR) accessory. High resolution mass spectra were recorded using a direct inlet system (ESI) in electrospray ionization mode.

### 4.2 *General procedure for the synthesis of conjugates hcptpyDP and hcptpyTP*

Acid hcptpy (1 eq), prepared according to reference 26(b), and FDPP (1.3 eq) were dissolved in DMF (20 mL/mmol of acid) and DIPEA (4 eq) was added under nitrogen atmosphere. After stirring for 10 min, the adequate amine (1 eq) in DMF (15 mL/mmol of acid) was added and the reaction was stirred at room temperature overnight. Then, the solution was washed with saturated $NaHCO_3$ (3 x) and brine. The organic phase was dried over $MgSO_4$, filtered and evaporated under reduced pressure to give a residue that was purified through silica gel column chromatography using mixtures of EtOAc and MeOH as the eluent to afford the corresponding product.

#### *4.2.1 Conjugate hcptpyDP*

Eluent: from EtOAc to EtOAc/MeOH 1:1; yield: 140 mg; 63%; white solid, mp (MeOH) 239 ºC (dec); $[\alpha]_D^{20}$ = +23 (c = 1.0, MeOH); IR: 3280, 2921, 2851, 2358, 1729, 1632, 1584, 1541 $cm^{-1}$; $^1H$ NMR ($CDCl_3$): δ 2.02 (m, 5H), 2.25-2.37 (m, 3H), 3.05 (m, 1H), 3.24 (m, 1H), 3.74 (s, 3H), 4.59 (m, 2H), 6.69 (m, 1H), 7.39 (m, 2H), 7.92 (m, 4H), 7.98 (m, 2H), 8.69 (m, 2H), 8.75 (m, 4H), 9.00 (m, 1H); $^{13}C$ NMR ($CDCl_3$): δ 18.7, 18.8, 24.4, 26.9, 46.6, 47.2, 48.7 49.6, 51.7, 118.8, 121.4, 124.0, 127.6, 133.4, 136.9, 142.2, 148.8, 149.1, 155.9, 156.1, 168.0, 172.0, 173.6; HRMS: Calculated for $C_{33}H_{31}N_5O_4Na$ ($M+Na^+$): 584.2268, Found 584.2259.

*4.2.2 Conjugate hcptpyTP*

Eluent: from EtOAc to EtOAc/MeOH 1:1; yield: 280 mg, 49%; white solid, mp (MeOH) 245 ºC (dec); $[\alpha]_D^{20}$ = -40 (c = 0.29, $CH_3OH$); IR: 3285, 2948, 1737, 1630, 1585 1537 $cm^{-1}$; $^1H$ NMR ($CDCl_3$): δ 1.92-2.06 (m, 2H), 2.23 (m, 4H), 2.47 (m, 2H), 3.30 (m, 1H), 3.43 (m, 1H), 3.73 (s, 3H), 3.82 (m, 2H), 4.05 (m, 1H), 4.21 (m, 1H), 4.68 (m, 1H), 4.99 (m, 1H), 6.44 (m, 1H), 6.48 (m, 1H), 7.06 (d, 1H), 7.36 (m, 2H), 7.80 (d, 1H), 7.88-7.93 (m, 6H), 8.65 (m, 2H), 8.72 (m, 4H); $^{13}C$ NMR ($CDCl_3$): δ 18.1, 18.9, 28.8, 29.4, 30.5, 41.3, 45.0, 45.4, 52.4, 118.8, 121.3, 123.9, 127.2, 127.9, 134.5, 136.9, 149.0, 149.3, 155.9, 171.1, 172.9; HRMS: Calculated for $C_{37}H_{37}N_7O_8Na$ ($M+Na^+$): 698.2698, Found 698.2702

*4.3 General procedure for the preparation of complexes [Ru(pydic)(hcptpyDP)] and [Ru(pydic)(hcptpyTP)]*

[Ru(*p*-cymene)$Cl_2$]$_2$ (0.5 eq) and the desired terpyridine conjugate (1 eq) were dissolved in MeOH (14 mL/mmol) under $N_2$ atmosphere. Sodium 2-pyridine-2,6-dicarboxylate (1 eq) was added in MeOH/$H_2O$, 2:1 (13 mL/mmol of pydic) and the whole reaction mixture was heated at 60 ºC for 1 h. After the reaction mixture was

cooled to r.t. and $CH_2Cl_2$ and $H_2O$ were added. The organic layer was separated and the aqueous layer was extracted with $CH_2Cl_2$ (3 x). The combined organic layer was dried over $MgSO_4$, filtered and evaporated under reduced pressure to give a residue that was purified through silica gel column chromatography using mixtures of $CH_2Cl_2$ and MeOH as the eluent to afford the corresponding product.

*4.3.1 Complex [Ru(pydic)(hcptpyDP)]*

Eluent**:** from $CH_2Cl_2$ to $CH_2Cl_2$/MeOH 100:5; yield: 70 mg, 60%; IR: 3261, 1725, 1615, 1540 $cm^{-1}$; $^1H$ NMR (DMSO-$d_6$): δ 1.78-1.99 (m, 5H), 2.12 (m, 3H), 3.12 (m, 2H), 3.58 (s, 3H), 4.34 (m, 1H), 4.53 (m, 1H), 6.84 (m, 1H), 7.46 (m, 1H), 7.57 (m, 2H), 7.78 (m, 1H), 7.91 (m, 1H), 8.00 (m, 2H), 8.10 (m, 2H), 8.20 (m, 2H), 8.34 (m, 3H), 8.87 (m, 2H), 8.95 (s, 2H); $^{13}C$ NMR (DMSO-$d_6$): δ 18.8, 18.9, 22.6, 26.0, 26.9, 29.2, 29.5, 45.8, 47.1, 47.4, 51.9, 119.4, 123.9, 124.1, 124.2, 127.4, 127.7, 128.5, 135.2, 138.3, 138.8, 139.2, 144.2, 150.6, 150.9, 160.4, 160.9, 165.6, 166.5, 171.5, 171.8, 173.6; HRMS: Calculated for $C_{40}H_{34}N_6O_8RuNa$ ($M+Na^+$): 851.1385, Found: 851.1384.

*4.3.2 Complex [Ru(pydic)(hcptpyTP)]*

Eluent**:** from $CH_2Cl_2$ to $CH_2Cl_2$/MeOH 100:5; yield: 28 mg, 54%; IR: 3385, 1733, 1599, 1541 $cm^{-1}$; $^1H$ NMR (DMSO-$d_6$): δ 1.84-2.29 (m, 8H), 3.01 (m, 1H), 3.23 (m, 1H), 3.53 (m, 2H), 3.60 (s, 3H), 3.83 (m, 2H), 4.50 (m, 1H), 4.80 (m, 1H), 6.88 (m, 1H), 7.52 (m, 2H), 7.61 (m, 1H), 7.81 (m, 2H), 7.96 (m, 2H), 8.05 (m, 2H), 8.19 (m, 2H), 8.34 (m, 3H), 8.51(m, 1H), 8.65 (m, 1H), 8.89-8.97 (m, 4H); $^{13}C$ NMR (DMSO-$d_6$): δ 18.8, 22.6, 27.0, 28.8, 29.0, 29.2, 29.3, 29.5, 31.8, 45.2, 52.2, 55.4, 119.4, 123.9, 124.1, 124.3, 127.3, 127.6, 127.8, 128.3, 135.5, 138.3, 138.8, 150.4, 150.6, 150.8, 160.4, 161.0, 168.5, 170.8, 171.0, 171.4, 171.5, 172.7, 173.1; HRMS: Calculated for $C_{44}H_{40}N_8O_{10}RuNa$ ($M+Na^+$): 965.1815, Found: 965.1824

*4.4 General procedure for catalyzed epoxidation reactions*

The desired complex (0.005 mmol, 0.005 eq) was sonicated in 10 mL of $CH_2Cl_2$/MeOH 9:1. Then, the olefin (1 mmol, 1 eq) and undecane (GC internal standard, 100 μL) were added. After, urea hydrogen peroxide complex (0.188 g, 2 mmol, 2 eq) was added in three portions at 0, 1 and 2 h. The reaction mixture was stirred at r.t. and aliquots were taken and subjected to GC analysis for the determination of yield data. When the reaction was finished, the suspension was washed successively with aqueous solutions of $NaHCO_3$ and brine. The organic layer was dried over $MgSO_4$, and the solvent was removed under reduced pressure. The corresponding epoxide was obtained without the need of further purification (see Supporting Data for details).

*4.5 Gas chromatography*

GC was performed using an apparatus equipped with FID detector. Samples were dissolved in $CH_2Cl_2$ and filtered through a microfilter. A capillary column (30 m x 250 mm x 0.25 mm) was used. Yields of the epoxidation reactions were determined using GC analysis. Calibrations using 5 standard samples containing different ratios of the corresponding epoxide product and undecane (internal standard) were performed. Yields of catalyzed reactions were calculated from the linear interpolation of the corresponding calibration function (see Supporting Data for details).

*4.6 Electrochemical studies*

Cyclic voltammetry (CV) and differential pulse voltammetry (DPV) experiments were performed on a potentiostat using three-electrode cell. A glassy carbon electrode (2 mm diameter) was used as working electrode, a platinum wire as auxiliary electrode, and a saturated calomel electrode (SCE) as a reference electrode. Complexes were dissolved in MeOH containing 0.1M of $TBABF_4$ as supporting electrolyte. $E_{1/2}$ values were determined as detailed in ESI.

*4.7 SEM Measurements*

SEM images were acquired with an apparatus equipped with a field emission gun. Wet gels were placed on a carbon-film-coated copper grid and dried by standing for 30 minutes on the grid. The resulting xerogels (dry gels) were then introduced into the microscope working at 60-80 Pa and 5 kV.

*4.8 CD measurements*

In the experiments in solution, the samples were dissolved in MeOH (0.05 mM) and the CD spectra were recorded using a 1 cm width quartz cuvette and were processed using the associated software. For the experiments in xerogel, first a gel at the *mgc* was prepared in toluene. Then the solvent of the gel was removed under vacuum to get the xerogel. Samples were prepared mixing the xerogels at around 0.020-0.025 mmol $g^{-1}$ with KBr (1.2-1.6 wt. %) in an agate mortar and pressing the mixture for 10 minutes. Translucent disks were obtained and the CD spectra were recorded using the same spectropolarimeter.

*4.9 Computational details*

Conformational searches were carried out using a mixed low mode/torsional sampling[32] with the OPLS-2005[33] force field implemented in the MacroModel[34] program to find and select an approximation of the most stable conformers. The geometries of the lowest energy conformers of the monomer of each compound were optimized using DFT calculations with the Gaussian09[35] program with the M06-2X[36] functional with the 6-31G(d) basis set. The most stable structures were also done for dimeric and tetrameric aggregates. The most stable structures were optimized at the M06-2X/6-31G(d) level of calculation. The dodecameric structure of hcptpyTP was constructed using the same methodology described for the dimer and the tetramer but in this case, only a minimization of the energy using molecular mechanics was carried out.

## Dedication

This paper is warmly dedicated to Professor Léon Ghosez, to honor his fruitful and long lasting compromise with the progress of chemical science.


## Acknowledgements

Financial support from Spanish MINECO (grant CTQ2016-77978-R) is gratefully acknowledged.


## Appendix A. Supplementary data

Supplementary data related to this article can be found at http:// dx.doi.org/xxxx. Aggregation energies for the formation of aggregates, DPV voltammograms of [Ru(pydic)(hcptpyDP)] and [Ru(pydic)(hcptpyTP)] and determination of $E_{1/2}$ values, UV spectra of hcptpyDP and hcptpyTP, $^{1}H$ and $^{13}C$ NMR spectra of the new products, experimental data from studies on the epoxidation of olefins, cartesian coordinates of monomers and aggregates of hcptpyDP and hcptpyTP.

## References


1. Morgan GT, Burstall FH. *J. Chem. Soc*. 1932: 20-30.
2. Tse MK, Jiao H, Anilkumar G, Bitterlich B, Gelalcha FG, Beller M. *J. Organomet.* 2006, 691: 4419-4433.
3. (a) Delgado J, Zhang Y, Xu B, Epstein IR. *J. Phys. Chem. A* 2011, 115: 2208–2215; (b) *Terpyridine-based Materials: for Catalytic, Optoelectronic, and Life-Science Applications*; Schubert, U.S.; Winter, A.; Newkome G.R., Eds.; Wiley-VCH: Weinheim, 2011.

4. (a) Constable EC. *Chem. Soc. Rev*. 2007, 36: 246-253; (b) Wild A, Winter A, Schlütter F, Schubert US. *Chem. Soc. Rev*. 2011, 40: 1459-1511.
5. See, for instance: (a) Trawick BN, Osiek TA, Bashkin JK. *Bioconjug. Chem*. 2001, 12: 900-905; (b) Putnam WC, Bashkin JK. *Nucleosides Nucleotides Nucleic Acids* 2005, 24: 1309-1323; (c) Graf N, Göritz M, Kramer R. *Angew. Chem. Int. Ed*. 2006, 45: 4013-4015; (d) Füssi A, Schleifenbaum A, Göritz M, Riddell A, Schultz C, Krämer R. *J. Am. Chem. Soc*. 2006, 128: 5986-5987.
6. Heinze K, Hempel K, Breivogel A. *Z. Anorg. Allg. Chem*. 2009, 635: 2541-2549.
7. Jarosz P, Du P, Schneider J, Lee S-H, McCamant D, Eisenberg R. *Inorg. Chem*. 2009, 48: 9353-9363.
8. Sil A, Giri D, Patra SK. *J. Mater. Chem*. C 2017, 5: 11100-11110.
9. Sasabe H, Hayasaka Y, Komatsu R, Nakao K, Kido J. *Chem. Eur. J*. 2017, 23: 114-119.
10. Martínez MA, Carranza MP, Massaguer A, Santos L, Organero JA, Aliende C, de Llorens R, Ng-Choi I, Feliu L, Planas M, Rodríguez AM, Manzano BR, Espino G, Jalón FA. *Inorg. Chem*. 2017, 56: 13679-13696.
11. Wang T, Li H. *Chem. Eur. J*. 2016, 22 : 12400-12405.
12. Dong D, Li Z, Yu N, Zhao H, Chen H, Liu J, Liu D. *New. J. Chem*. 2018, 42: 9317-9323.
13. Yuan D, Zhang YD, Jiang ZW, Peng ZW, Huang CZ, Li YF, *Mater. Lett.* 2018, 211: 157-160.
14. For a general and recent review on this area, see: Amabilino DB, Smith DK, Steed JW. *Chem. Soc. Rev*. 2017, 46: 2404-2420.
15. For a recent book on organogels, see: Guenet JM in *Organogels – Thermodynamics, Structure, Solvent Role, and Properties*; Springer, 2016.

16. See, for instance: (a) Van Esch JH, Feringa BL. *Angew. Chem. Int. Ed.* 2000, 39: 2263-2266; (b) Steed W. *Chem. Commun.* 2011, 47: 1379–1383.

17. For some examples, see: (a) Fernández-Barbero A, Suárez IJ, Sierra-Martín B, Fernández-Nieves A, de las Nieves FJ, Marquez M, Rubio-Retama J, López-Cabarcos E. *Adv. Colloid Interface Sci*. 2009, 147-148: 88–108; (b) Smith DK. *Chem. Soc. Rev.* 2009, 38: 684-694; (c) Duan P, Cao H, Zhang L, Liu M. *Soft Matter* 2014, 10: 5428-5448.

18. Okesola BO, Smith DK, *Chem. Soc. Rev*. 2016, 45: 4226-4251.

19. (a) Prathap A, Sureshan KM. *Angew. Chem. Int. Ed*. 2017, 56: 9405-9409; (b) Raju CSK, Pramanik B, Ravishankar R, Rao PVC, Sriganesh G. *RSC Adv*. 2017, 7: 37175-37180.

20. (a) Rúa F, Boussert S, Parella T, Diez-Pérez I, Branchadell V, Giralt E, Ortuño RM. *Org. Lett*. 2007, 9: 3643-3645; (b) Torres E, Gorrea E, Burusco KK, Da Silva E, Nolis P, Rúa F, Boussert S, Díez-Pérez I, Dannenberg S, Izquierdo S, Giralt E, Jaime C, Branchadell V, Ortuño RM, *Org. Biomol. Chem*. 2010, 8: 564-575.

21. Gorrea E, Nolis P, Torres E, Da Silva E, Amabilino DB, Branchadell V, Ortuño RM. *Chem. Eur. J*, 2011, 17: 4588-4597.

22. Celis S, Nolis P, Illa O, Branchadell V, Ortuño RM. *Org. Biomol. Chem.* 2013, 11: 2839-2846.

23. Pi-Boleda B, Sans M, Campos M, Nolis P, Illa O, Estévez JC, Branchadell V, Ortuño RM. *Chem. Eur. J.* 2017, 23: 3357-3365.

24. Torres E, Gorrea E, Da Silva E, Nolis P, Branchadell V, Ortuño RM. *Org. Lett.* 2009, 11: 2301-2304

25. Celis S, Gorrea E, Nolis P, Illa O, Ortuño RM. *Org. Biomol. Chem.* 2012**,** 10: 861-868.

26. (a) Constable EC, Dunphy EL, Housecroft CE, Neuburger M, Schaffner S, Schaper F, Batten SR. *Dalton Trans*. 2007: 4323-4332; (b) Ashford DL, Song W, Concepcion JJ, Glasson CRK, Brennaman MK, Norris MR, Fang ZF, Templeton JL, Meyer TJ. *J. Am. Chem. Soc.* 2012, 134: 19189-19198.

27. Norrby T, Börje A, Åkermark B, Hammarström L, Alsins J, Lashgari K, Norrestam R, Mårtensson J, Stenhagen G. *Inorg. Chem.* 1997, 36: 5850–5858.

28. Gorrea E, Pohl G, Nolis P, Celis S, Burusco KK, Branchadell V, Perczel A, Ortuño RM. *J. Org. Chem*. 2012, 77: 9795-9806.

29. (a) de Loos M, van Esch J, Kellogg RM, Feringa BL. *Angew. Chem. Int. Ed.* 2001, 40: 613-616; (b) Hunter CA, Anderson HL. *Angew. Chem. Int. Ed.* 2009, 48: 7488–7499; (c) Hirst AR, Coates IA, Boucheteau TR, Miravet JF, Escuder B, Castelletto V, Hamley IW, Smith DK *J. Am. Chem. Soc.* 2008, 130: 9113–9121; (d) Mahadevi AS, Sastry GN *Chem. Rev.* 2016, 116: 2775–2825.

30. (a) Zhou P, Zhao N, Rele DN, Berova N, Nakanishi K. *J. Am. Chem. Soc*. 1993, 115: 9313-9314; (b) Pesticelli G, Di Bari L, Berova N. *Chem. Soc. Rev*. 2011, 40: 4603-4625.

31. (a) Iavicoli P, Xu H, Feldborg LN, Linares M, Paradinas M, Stafström S, Ocal C, Nieto-Ortega B, Casado J, Navarrete JTL, Lazaroni R, de Feyte S, Amabilino DB. *J. Am. Chem. Soc.* 2010, 132: 9350–9362; (b) Würthner F, Kaiser TE, Saha-Möller CR. *Angew. Chem. Int. Ed.* 2011, 50: 3376–3410.

32. Kolossváry I, Guida WC. *J. Am. Chem. Soc.* 1996, 118: 5011–5019.

33. Kaminski GA, Friesner RA, Tirado-Rives J, Jorgensen WL. *J. Phys. Chem. B* 2001, 105: 6474–6487.

34. Mohamadi F, Richards NGJ, Guida WC, Liskamp R, Lipton M, Caufield C, Chang G, Hendrickson T, Still WC. *J. Comput. Chem.* 1990, 11: 440–467.

35. Gaussian 09, Revision C.01, Frisch MJ, Trucks GW, Schlegel HB, Scuseria GE, Robb MA, Cheeseman JR, Scalmani G, Barone V, Mennucci B, Petersson GA, Nakatsuji H, Caricato M, Li X, Hratchian HP, Izmaylov AF, Bloino J, Zheng G, Sonnenberg JL, Hada M, Ehara M, Toyota K, Fukuda R, Hasegawa J, Ishida M, Nakajima T, Honda Y, Kitao O, Nakai H, Vreven T, Montgomery, Jr. JA, Peralta JE, Ogliaro F, Bearpark M, Heyd JJ, Brothers E, Kudin KN, Staroverov VN, Kobayashi R, Normand J, Raghavachari K, Rendell A, Burant JC, Iyengar SS, Tomasi J, Cossi M, Rega N, Millam JM, Klene M, Knox JE, Cross JB, Bakken V, Adamo C, Jaramillo J, Gomperts R, Stratmann RE, Yazyev O, Austin AJ, Cammi R, Pomelli C, Ochterski JW, Martin RL, Morokuma K, Zakrzewski VG, Voth GA, Salvador P, Dannenberg JJ, Dapprich S, Daniels AD, Farkas Ö, Foresman JB, Ortiz JV, Cioslowski J, Fox DJ. Gaussian, Inc., Wallingford CT, 2009. http://www.gaussian.com

36. Zhao Y, Truhlar DG. *Theor. Chem. Acc.* 2007, 120: 215–241.